



MURDOCH RESEARCH REPOSITORY

<http://researchrepository.murdoch.edu.au>

This is the author's final version of the work, as accepted for publication following peer review but without the publisher's layout or pagination.

Kala, J. , Lyons, T.J. and Nair, U.S. (2011) Numerical simulations of the impacts of land-cover change on cold fronts in South-West Western Australia. *Boundary-Layer Meteorology*, 138 (1). pp. 121-138.

<http://researchrepository.murdoch.edu.au/3668>

Copyright © 2010 Springer Science+Business Media B.V.
It is posted here for your personal use. No further distribution is permitted.

Numerical Simulations of the Impacts of Land-Cover Change on Cold Fronts in South-West Western Australia

J. Kala · T. J. Lyons · U. S. Nair

Received: date / Accepted: date

Abstract The south-west of Western Australia has experienced significant land-cover change as well as a decline in rainfall. Given that the majority of precipitation results from frontal passages, the impact of land-cover change on the dynamics of cold fronts is explored using the Regional Atmospheric Modelling System version 6.0. Frontal simulations are evaluated against high resolution atmospheric soundings, station observations, and gridded rainfall analyses and shown to reproduce the qualitative features of cold fronts. Land-cover change results in a decrease in total frontal precipitation through a decrease in turbulent kinetic energy and vertically integrated moisture convergence, and an increase in wind speed within the lower boundary layer. Such processes contribute to reduced convective rainfall under current vegetation.

Keywords Cold front · Land-atmosphere interactions · Land-cover change · Regional Atmospheric Modelling System

J. Kala and T. J. Lyons
School of Environmental Science
Murdoch University
South Street, Murdoch
6150 WA, Australia
Tel.: +61-08-93602737
Fax: +61-08-93104997
E-mail: J.Kala@murdoch.edu.au
E-mail: T.Lyons@murdoch.edu.au

U. S. Nair
Earth System Science Center
National Space Science and Technology Center
University of Alabama in Huntsville,
Alabama, USA 35806

T. J. Lyons and U. S. Nair
Centre of Excellence for Climate Change Woodland and Forest Health
<http://www.foresthealth.com.au/index.php>

1 Introduction

The south-west of Western Australia (SWWA) (Fig. 1) is typified by a Mediterranean climate with cool, wet winters and warm, dry summers (Gentili 1971). Most of the rain occurs in winter (May to October) and is brought about by cold fronts and cloud bands (IOCI 2002). The formation of fronts is mainly driven by the interaction of sub-tropical and polar air which provides the conditions for a continual cycle of frontal development within the prevailing westerlies (Sturman and Tapper 1996). Namely, fronts develop along troughs in-between the anticyclonic cells of the sub-tropical high pressure belt. In winter, these fronts frequently travel across SWWA and result in precipitation events, and in summer, the frequency of fronts traveling across SWWA decreases as the sub-tropical highs (anticyclones) move further south.

The first comprehensive study of frontal systems and winter rainfall over SWWA was by Wright (1974) who identified two major rainfall types. He describes the first type of winter rain as originating from strong north-westerly winds associated with the approach of cold fronts advecting relatively warm humid air from the southern Indian Ocean. He argues that these occur in early winter (May to July), are strongly linked to the oscillation of the sub-tropical highs, and are not strongly impacted by coastal orography and surface friction. Type 2 rainfall occurs mostly in late winter (August to October) and is associated with convection during or after the passage of a cold front. Wright (1974) argues that this type is not as strongly related to general circulation features, i.e., the subtropical highs, and is enhanced by coastal friction and orography.

Following the work of Wright (1974), a significant decline in winter rainfall was noticed in the 1970s, which has persisted since then (IOCI 2002). This has resulted in a significant body of research into the likely causes of this decline and a comprehensive review can be found in Bates et al. (2008). As a brief summary, this extensive literature can be broadly classified into two major categories. The first is that the decline in rainfall is directly linked to changes in the large scale synoptic features of the southern hemisphere such as patterns of mean sea level pressure and sea surface temperatures (e.g., Allan and Haylock 1993; Smith et al. 2000; England et al. 2006; Hope et al. 2006; Samuel et al. 2006; Nicholls 2010). One of the over-arching arguments is that the frequency of synoptic features leading to winter rainfall, i.e., troughs and cold fronts, have shown a marked decline, while the frequency of high-pressure cells over the continent (and associated drier conditions) has increased. This change in dominant synoptic features has been linked to the increasing level of greenhouse gases (Hope et al. 2006; Cai and Cowan 2006).

The second school of thought is that land-cover change via the large-scale clearing of native vegetation for agriculture in SWWA has altered the boundary layer dynamics of the region and can explain at least part of the observed decline in rainfall. The extent of land-cover change in SWWA is illustrated in Fig. 1 showing the vermin fence acting as a clear boundary between undisturbed native vegetation east of the fence and agricultural land west of the fence (shaded), representing an estimated 13 million hectares of native perennial vegetation cleared since European settlement (Huang et al. 1995). The impacts of land-cover change were first investigated by Lyons et al. (1993) and Lyons (2002) who used aircraft and surface measurements to

show that the reduced albedo, higher roughness length and canopy resistance over the native vegetation results in higher sensible heat fluxes and hence enhances convective cloud formation especially during spring months. Pitman et al. (2004) further investigated the impacts of land-cover change on the July climate of SWWA by running 3 regional climate models at a $50 \text{ km} \times 50 \text{ km}$ resolution using current as well as Pre-European (pristine) vegetation cover. All 3 models showed a decrease in rainfall with the current vegetation, which was attributed to a reduction in surface roughness and frictional drag by the removal of native vegetation. They argued that land-cover change lead to increased divergence of moisture advected from the Indian Ocean at the coast and an increased convergence and higher vertical velocities further inland. This was related to the observed increase in rainfall inland and decrease closer to the coast and hence, Pitman et al. (2004) argue that land-cover change provides a plausible mechanism to explain at least some of the decrease in winter rainfall.

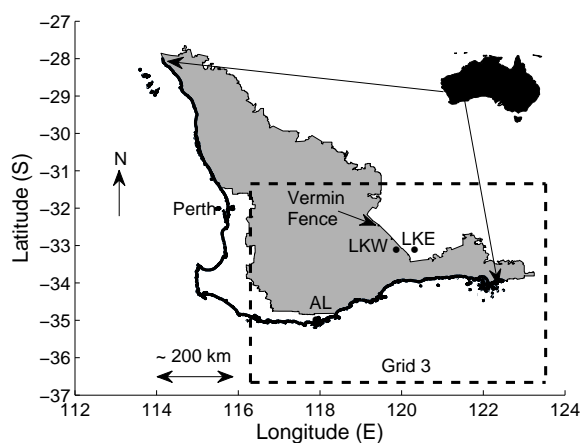


Fig. 1 Map showing the vermin fence acting as a boundary between agricultural land use (shaded), west of the fence, and native vegetation, east of the fence, in south-west Western Australia (SWWA). The map shows the release locations of the atmospheric soundings at the Lake King East (LKE) and Lake King West (LKW) sites, the location of the meteorological station at Albany Airport (AL), and the boundary of Grid 3.

The interaction between vegetation and the atmosphere has also been extensively studied elsewhere. Anthes (1984) postulated that vegetation bands of up to 50-100 km in semiarid regions could potentially initiate and enhance moist convection under the appropriate atmospheric conditions. More realistic numerical simulations by Pielke et al. (1999) have shown that landscape (vegetation) changes in Florida between 1900 and 1993 can account for up to an 11 % decrease in summer rainfall in this region and Kanae et al. (2001) found similar effects for September rainfall on the Indochina peninsula. A comprehensive review of the effects of land-cover change on atmospheric circulations can be found in Pielke (2001), Pielke et al. (2007), and Cotton and Pielke (2007).

In summary, there is ample evidence that land-atmosphere interactions are an important part of the overall hydrological cycle. Although the work of Pitman et al. (2004) provides useful insight into land-atmosphere interactions and precipitation, it did not explicitly focus on the interaction between cold fronts (a major source of precipitation) with the land surface in SWWA. The ongoing *bufex* field campaign (Lyons et al. 1993) recently completed the collection of high resolution atmospheric soundings in SWWA during December 2005 (summer) and August 2007 (late winter to early spring), during which two cold fronts were observed to travel across SWWA and resulted in precipitation events. Accordingly, the aim of this paper is to investigate the interactions of these two cold fronts with the land surface. Numerical experiments are carried out with RAMS (Pielke et al. 1992; Cotton et al. 2003) (latest version 6.0) and the model is evaluated against the high resolution atmospheric soundings, as well as station observations and grided rainfall analyses. Sensitivity tests are carried out to investigate the impacts of historical land-cover change on the structure and dynamics of the cold fronts.

2 Study area and field data

Field observations were undertaken in December 2005 and August 2007. December is during the austral summer season, with the agricultural region being bare of crops following harvest and covered with harvest stubbles approximately 0.2 m high or bare soil and August is during late winter to early spring, with the agricultural region active. The native vegetation east of the fence (Fig. 1) is undisturbed and in its pristine state. It is mostly comprised of *eucalyptus eremophilla* species and patches of eucalypt woodland can be found on the lower ground and *casuarina* thickets on the residual plateau soils (Lyons et al. 1996). The height of the native trees varies between 0.5 m to 6.0 m and more than 75% are between 0.5 m and 2.0 m high (Esau and Lyons 2002). There is no irrigation across the region and the overall landscape inland is flat. The predominant soil type is a duplex soil of sand over clay.

High resolution atmospheric soundings were acquired using the National Center for Atmospheric Research Mobile Global Positioning System Advanced Upper-Air Sounding System during the first three weeks of December 2005 and August 2007 at 3-hourly intervals at two locations near the town of Lake King, namely, the Lake-King West (LKW) and Lake-King East (LKE) sites respectively (Fig. 1). The soundings provided profiles of temperature, relative humidity, wind speed and direction either side of the vermin fence (i.e., the LKW site in the agricultural region and the LKE site in the native vegetation) from the surface to about 12 km. This data were collected as part of the ongoing *bufex* field campaign (Lyons et al. 1993) and all soundings were subjected to data quality control. These soundings were not assimilated into RAMS but used to evaluate the model.

The Australian Bureau of Meteorology operates a large number of automated meteorological stations across SWWA which record hourly data including temperature, wind speed, wind direction, relative humidity, and pressure. Data from the Albany Airport station (AL in Fig. 1) were used to compared against the model. The bu-

reanu also provides gridded analyses of daily precipitation over Australia at a 5 km resolution. These analyses were used to compare against the simulated precipitation.

3 Model description and initialization

RAMS is a highly versatile three-dimensional mesoscale meteorological model (Pielke et al. 1992; Cotton et al. 2003) that has been extensively used for a wide variety of applications including modelling sea breezes (e.g., Ma and Lyons 2000; Cai and Steyn 2000; Miao et al. 2003; Kala et al. 2010) and storm events (e.g., Nair et al. 1997; Kotroni et al. 1998; Ryan et al. 2000; Gero and Pitman 2006). The latest 6.0 version was utilised and operated as a non-hydrostatic, compressible, primitive equation model with a σ_z terrain-following vertical coordinate system with polar stereographic coordinates. RAMS 6.0 is coupled to a Land-Ecosystem Atmosphere Feedback Model (LEAF-3) that represents the energy and moisture budgets at the surface and their interactions with the atmosphere (Walko et al. 2000). It incorporates the interactions between soil and vegetation and the atmosphere at a sub grid scale; see Walko et al. (2000) for detailed model descriptions.

Three nested grids were used with Grid 1 covering the Australian continent and its contiguous Indian and Southern oceans at a grid spacing of $60 \text{ km} \times 60 \text{ km}$ and covering a domain of $3180 \text{ km} \times 2580 \text{ km}$, Grid 2 had a spacing of $20 \text{ km} \times 20 \text{ km}$ and domain of $1420 \text{ km} \times 1240 \text{ km}$, and Grid 3 a spacing of $5 \text{ km} \times 5 \text{ km}$ and domain of $650 \text{ km} \times 590 \text{ km}$ (Fig. 1). 28 vertical levels were used for each grid starting at 20 m above ground level to 21 km, with the lower levels having higher resolution and the upper levels were gradually stretched to a maximum spacing of 2 km in the upper levels of the atmosphere and 10 soil layers were used. The turbulence closure scheme of Mellor and Yamada (1982) was used for vertical diffusion and horizontal diffusion was taken as proportional to the horizontal deformation rate with a coefficient based on the Smagorinsky (1963) formulation. The Harrington scheme (Harrington 1997) was used for longwave and shortwave radiation and the Kain-Fritsch convective parameterization scheme (Kain and Fritsch 1993) was utilized in the two outer grids and explicit microphysical parameterization (Walko et al. 1995; Meyers et al. 1997) was activated in all model grids.

RAMS was initialised with the $1^\circ \times 1^\circ$ National Center for Environmental Prediction Final Analyses at 6-hourly intervals. The model was nudged towards the lateral and top boundaries of the coarsest grid domain with no nudging in the centre of the domain. Soil moisture data from the Australian Soil Water Availability Project (Raupach et al. 2008; Raupach et al. 2009) were used for soil moisture initialisation. This data provides monthly means of upper (surface to 0.2 m) and lower (0.2 m to 1.5 m) relative soil moisture (percentage of field capacity) across the Australian continent at a $5 \text{ km} \times 5 \text{ km}$ grid spacing. The upper and lower layer soil moisture from this dataset were used to initialize the top three and bottom seven soil layers in RAMS respectively. The model was initialised 15 days prior to the event to allow for sufficient spin up of the soil variables and only two grids were used for computational efficiency. The model was then restarted with three grids by interpolating the soil variables from the spin-up run and the model was integrated for 72 hours

to capture the movement of the cold fronts across SWWA (i.e., 24 hours before the cold front reached the coast, 24 hours while it moved across, and 24 hours to capture post-frontal processes).

All input geographical datasets were obtained from the RAMS source distribution except that the mean sea surface temperatures for December 2005 and August 2007 were obtained from the National Oceanographic and Atmospheric Administration Optimum Interpolation Sea Surface Temperature V2 data archive (Reynolds et al. 2002), 9 s (≈ 250 m) topography was obtained from Geoscience Australia (Hutchinson et al. 2009), and the land-cover / vegetation classes were obtained from the Australian Surveying and Land Information Group (AUSLIG 1990). This data provides two vegetation datasets over the Australian continent, a current Post-European settlement vegetation cover dataset representative of 1988, and a Pre-European settlement vegetation cover dataset representative of 1788, and have been used previously in RAMS (e.g., Pitman et al. 2004; Peel et al. 2005; Kala et al. 2010). Following Kala et al. (2010), these vegetation classes were mapped to the LEAF-3 classes by mapping the vegetation data for the current vegetation types as close as possible to the vegetation files provided with the RAMS source distribution. Additionally, the data for current vegetation were modified to have bare soil, rather than crops within the agricultural region for December, as harvest had been completed by then. The same translation was used to convert the Pre-European vegetation data to LEAF-3 classes, and this dataset was used to carry out simulations of the effects of changes in land-cover. Hence in December, land-cover change represents a change from wooded grasslands to bare soil, whereas in August, it represents a change from wooded grasslands to crops.

4 Description of cold fronts and model evaluation

The two cold fronts were chosen based on days for which upper air observations were available for validation during December 2005 and August 2007, rather than the strongest cold fronts observed during these months. The summer cold front travelled across SWWA between the 10 and 11 December 2005 and the winter cold front between the 5 and 6 August 2007. This is illustrated in Fig. 2 showing the surface analysis chart at 0000 UTC (0800 LST) on 11 December 2005 and 0600 UTC (1400 LST) on 6 August 2007 respectively. Fig. 2a shows the summer front moving across SWWA, with cold air emanating from a low pressure cell in the southern Indian Ocean, and warmer air from the weak surface low and inland trough. The movement of the cold front is enhanced by the trough and the front eventually moves further south as the low pressure cell in the southern Indian Ocean weakens. Such a synoptic pattern is atypical for summer in SWWA, as the high pressure cells (anticyclones) associated with the sub-tropical high pressure belt are usually further south and cold fronts emanating from the cyclonic cells in the southern Indian Ocean seldom reach the coast. Fig. 2b on the other hand shows a typical winter pattern with high pressure cells located around 25°S in the eastern Indian Ocean and the central Australian continent respectively, with the cold front in the middle. The front reaches further north and the pressure gradient force is higher as compared to the summer case (Fig. 2a).

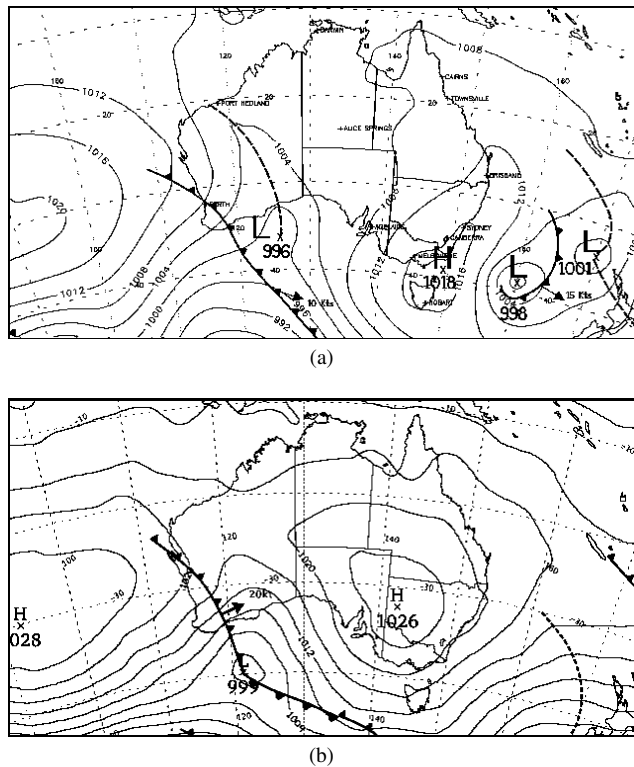


Fig. 2 Surface analysis charts for (a) the summer front at 0000 UTC (0800 LST) on 11 December 2005, and (b) the winter front at 0600 UTC (1400 LST) on 6 August 2007. Mean sea-level pressure contours are thin solid black lines, H denotes a high-pressure system (anticyclone), L denotes a low-pressure system (cyclone), and the thick solid black line with triangles illustrates the position cold front.

The passage of a cold front usually results in a sharp decrease in surface pressure and temperature due to the advection of moister, cooler maritime air, as well as an increase in moisture content and cloudiness. This is illustrated in Figs. 3 and 4 showing the observed and modelled time-series of sea-level pressure, temperature, mixing ratio (derived from the observed pressure, temperature, and relative humidity), wind speed, and wind direction at the AL station (Fig. 1) for the summer and winter fronts respectively. We note that the modelled temperature and wind speed have been corrected to screen level using surface-layer scaling, while the mixing ratio and wind direction are for the lowest grid (6.52 m). Figs. 3a and 4a show that the model clearly captures the decrease in sea-level pressure associated with the passage of the front and the subsequent increase as the front travels further east. However, the model performs poorly in reproducing the temperature trends, with over-predictions by as much as 5 °C (Figs. 3b and 4b). Namely, the model produces a normal temperature diurnal-cycle, while the data show evidence of rapidly changing cloudiness, as shown by the “kinks” in the temperature trace, which are not captured by the model. This is clearly evident in Fig. 4b between 0900 and 2100 LST on the 6 August 2007, with

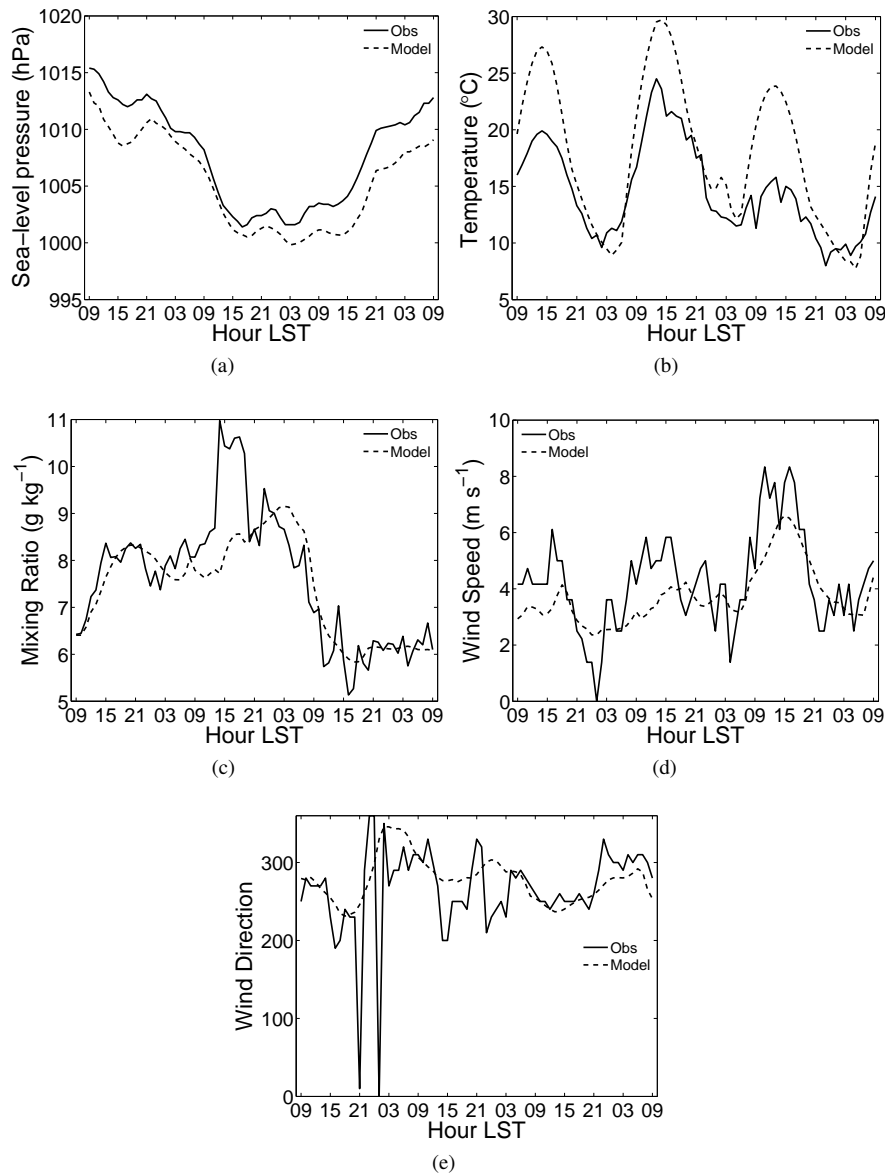


Fig. 3 Modelled and observed (Obs) time series of (a) sea-level pressure (hPa), (b) temperature ($^{\circ}\text{C}$), (c) mixing ratio (g kg^{-1}), (d) wind speed (m s^{-1}), and (e) wind direction at AL (Fig. 1) for the summer front from 0900 LST on the 9 December to 0900 LST on the 12 December 2005.

the observed temperature trace essentially lacking a daytime-maxima due to the passage of the front and associated cloudiness (other stations showed the same trends). This discrepancy can partly be explained by the fact that the model is initialised with boundary conditions at a resolution of one degree ($\approx 100 \text{ km}$), while the temperature

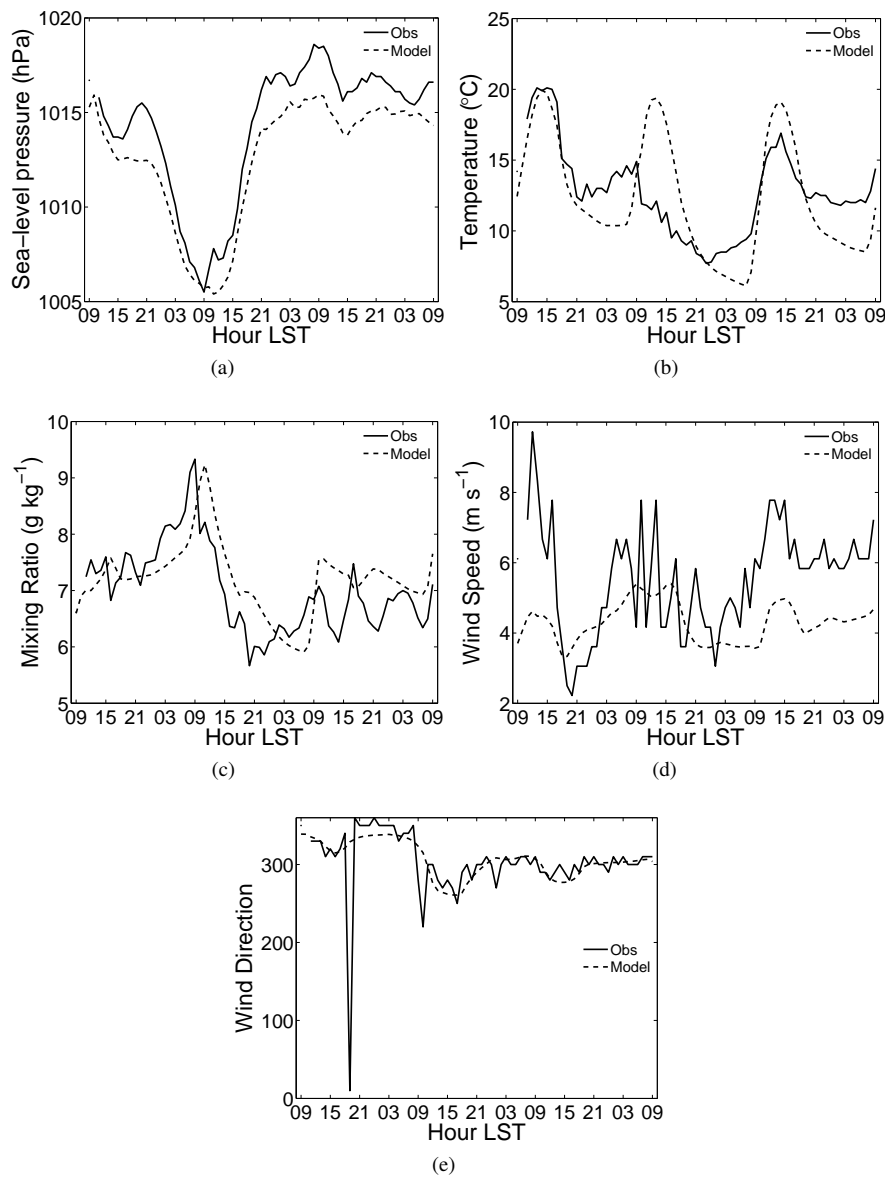


Fig. 4 Same as in Fig. 3 except for the winter front from 0900 LST on the 5 August to 0900 LST on the 8 August 2007.

contrast between warm and cold air at the frontal boundary is over a much smaller spatial scale. Hence, this sharp contrast in temperature is unlikely to be reproduced by the model (under its current configuration) and can partly explain temperatures being over-predicted. Nonetheless, Figs. 3c and 4c show that the model captures the

increase in mixing ratio associated with the passage of the front reasonably well, and wind speeds and wind direction are also reasonably well reproduced (Figs. 3d, e and 4d, e). We note that Fig. 3c shows a sharp increase in humidity between 1200 LST and 1500 LST on 10 December 2005, suggesting the arrival of a sea-breeze. While the model also shows an increase in mixing ratio over this period, the magnitude of the increase is small compared to the observations. Previous sea-breeze modeling in SWWA (Kala et al. 2010) has shown that RAMS tends to reproduce the qualitative features of the sea-breeze, while the quantitative errors can be large, i.e., the simulated sea-breeze is weaker than observed.

While Figs. 3 and 4 provide useful insight into the performance of the model close to the surface, it is equally important to examine the vertical structure of the atmosphere. This is illustrated in Fig. 5 showing the observed and modelled profiles of temperature, mixing ratio, wind speed and direction at the LKW site (Fig. 1) for the summer front on the 11 and 12 December 2005 at 0600 LST. The figure shows that the model reproduces the overall vertical structure of the atmosphere well. However, we note that the front reached the LKW and LKE sites close to 0900 LST on the 11 December, and since no soundings were available at that time, it is not possible to comment on the ability of the model to simulate the frontal passage. Nonetheless, Fig. 5 still provides some confidence in the model.

Fig. 6 shows the same variables plotted at the LKW site (Fig. 1) for the winter front on the 6 August 2007 at 1200 LST and 1500 LST respectively (the front reached the LKW and LKE sites between these times). The figure shows that the model performed reasonably well at 1200 LST, but did not capture the sharp decrease in temperature by as much as 5-8 °C at 1500 LST. This decrease in temperature is associated with the baroclinic zone at the frontal boundary which is substantially smaller as compared to the model grid spacing and input boundary conditions, and appears to have been smoothed out. Fig. 6b shows that the mixing ratio was generally over-predicted at 1500 LST, which can be related to temperatures being over-predicted. Fig. 6c shows that wind speeds were generally under-predicted at 1500 LST and the simulated wind direction (Fig. 6d) was off by about 30°. In general, comparison with the soundings further illustrates that the model does not capture the fine-scale structure of the front (comparison with soundings at the LKE site showed the same trends and have not been reproduced here for simplicity).

It is also important to evaluate the model's ability to simulate precipitation since the focus of this paper is on the effects of land-cover change on precipitation. Given that precipitation is highly variable and only resolved on the outer two grids (since the convective scheme is only valid for the first two grids), a direct comparison with station observations is difficult. However the Australian Bureau of Meteorology provides daily analyses of grided rainfall over Australia based on station observations, giving both the magnitude and spatial extent of precipitation. This is compared to the model output from grid 2 as illustrated in Figs. 7 and 8 showing the observed and simulated total surface accumulated precipitation for the summer and winter fronts respectively. Fig. 7 shows that the model reproduced the magnitude and spatial extent of precipitation reasonably well for the summer front, with precipitation generally under-predicted in the central and southern wheat-belt. Fig. 8 on the other hand shows that the model under-predicted precipitation along the west-coast and over-predicted

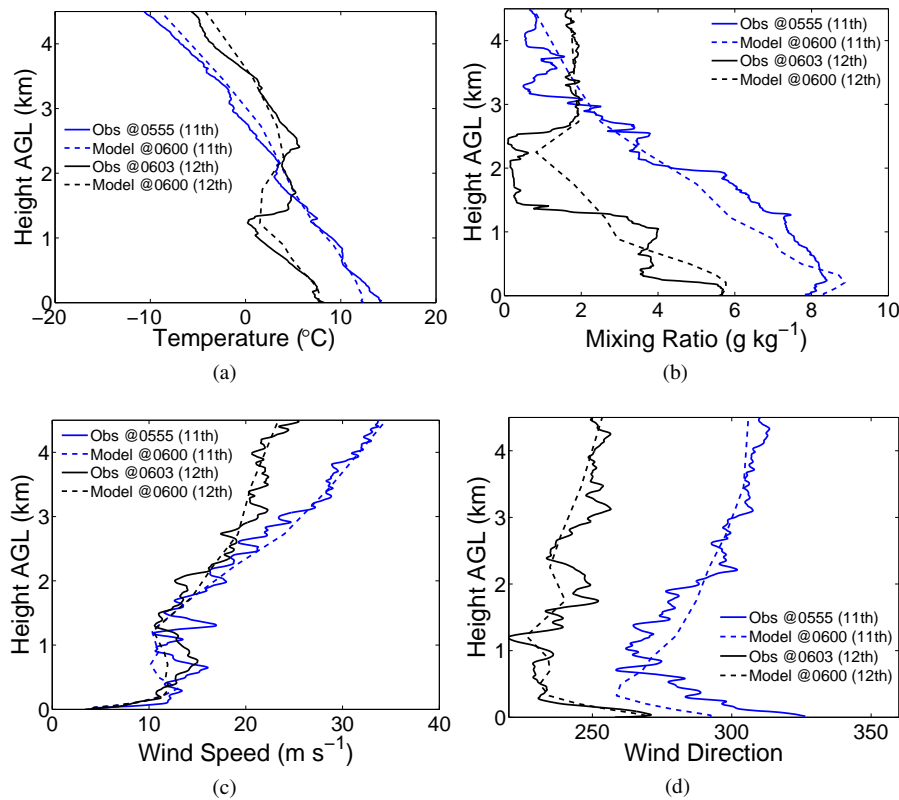


Fig. 5 Modelled and observed (Obs) profiles of (a) temperature ($^{\circ}\text{C}$), (b) mixing ratio (g kg^{-1}), (c) wind speed (m s^{-1}) and, (d) wind direction at the LKW site (Fig.1) for the summer front on the 11 and 12 December 2005 at 0600 LST.

precipitation in the eastern wheat-belt for the winter front. A possible explanation for the under-prediction along the west coast can be attributed to the Darling Scarp, a topographical feature of SWWA. The scarp can be observed from space, extending 200 km in a north-south direction from 31°S to 34°S (Fig. 1) roughly 25 km from the coast, representing a sudden increase in topography of about 300 m from sea level (Pitts and Lyons 1989). Pitts and Lyons (1990) used an earlier version of RAMS to model flows along the scarp and found that a horizontal resolution of 0.5 km was required to adequately simulate the meteorological impact of the scarp. These features are not resolved with a 20 km grid resolution and suggest that any topographical enhancement of precipitation would not be simulated. We note that this is an inherent limitation of the model as the convective scheme used assumes a horizontal grid spacing greater than 20 km.

Overall, comparison of the model output with station observations and the soundings show that the model captures the broad features of the front, but not the fine scale structure. Comparison with gridded rainfall observations show that coastal orographic effects are not well represented for the winter front, due to the coarse resolution of

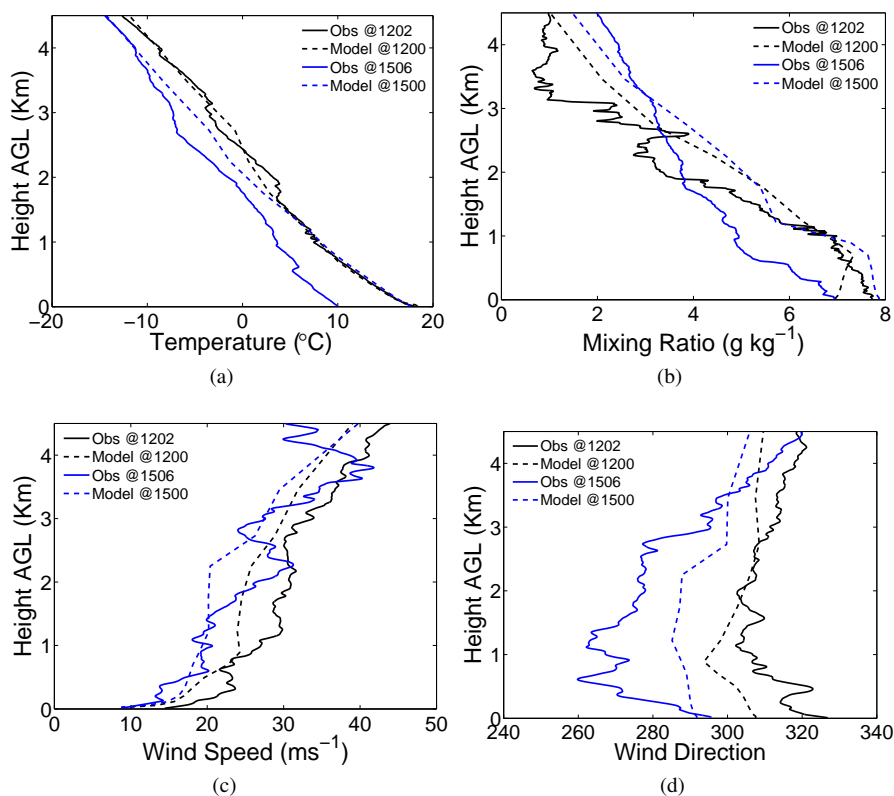


Fig. 6 Same as in Fig. 5 except for the winter front on the 6 August 2007 at 1200 LST and 1500 LST respectively.

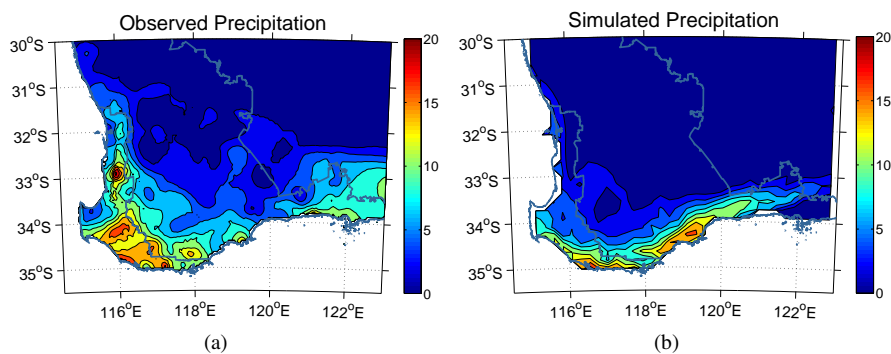


Fig. 7 (a) Observed and (b) simulated (Grid 2) total surface accumulated precipitation (mm) for the summer front, integrated from 0900 LST on the 9 December to 0900 LST on the 12 December 2005.

Grid 2. We note that several studies have used RAMS to model storm events, including those induced by cold fronts (Nair et al. 1997; Gero et al. 2006; Gero and Pitman

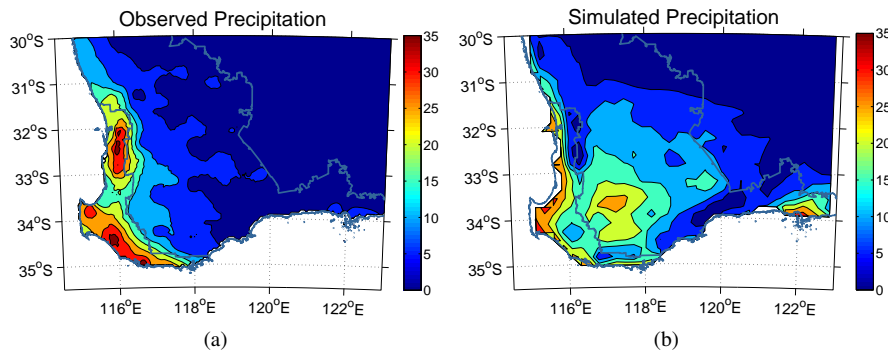


Fig. 8 Same as in Fig. 7 except for the winter front, integrated from 0900 LST on the 5 August to 0900 LST on the 8 August 2007.

2006). However, the latter do not evaluate the model output against observations, and hence, it is difficult to benchmark our results against similar studies. In fact, Gero and Pitman (2006) argue that they do not expect RAMS (when initialised with re-analysis data) to be able to reproduce a meteorological event on a particular day, since Australia is a relatively data-poor region (as compared to the United States), and hence, they do not evaluate their results against observations.

Having adequately evaluated the model, the next section discusses the impacts of land-cover change on cold-front dynamics.

5 Impacts of land-cover change

Figs. 9 and 10 show the difference in total surface accumulated precipitation between current and pre-European vegetation cover for the summer and winter fronts respectively, expressed in absolute values (rounded to the nearest mm) and as a percentage change (ΔP) respectively:

$$\Delta P = \left(\frac{P_{current} - P_{preEu}}{P_{current}} \right) \times 100 \quad (1)$$

where $P_{current}$ and P_{preEu} are the total surface accumulated precipitation (mm) under current and pre-European vegetation cover respectively (We note that ΔP will be greater than $\pm 100\%$ when the magnitude of the difference between $P_{current}$ and P_{preEu} is greater than $P_{current}$).

Fig. 9a shows a reduction in precipitation of up to 2-6 mm in the southern wheat-belt for the summer front, which corresponds to a percentage change of 50-150% (Fig. 10a). Fig. 9b shows a reduction of 2-4 mm across most of the wheat-belt for the winter front corresponding to a percentage change of approximately 50% (Fig. 10b). We note that these percentages need to be interpreted with care, namely a small absolute change in precipitation can represent a high percentage change (e.g., 1 mm to 2 mm, represents a 100% decrease under current vegetation, but is nonetheless a small absolute change). These are inherent limitations of doing single rather than

ensemble simulations, and hence, the focus of our paper is to explain the mechanisms behind the overall decrease in precipitation under current vegetation, rather than the magnitude of the decrease.

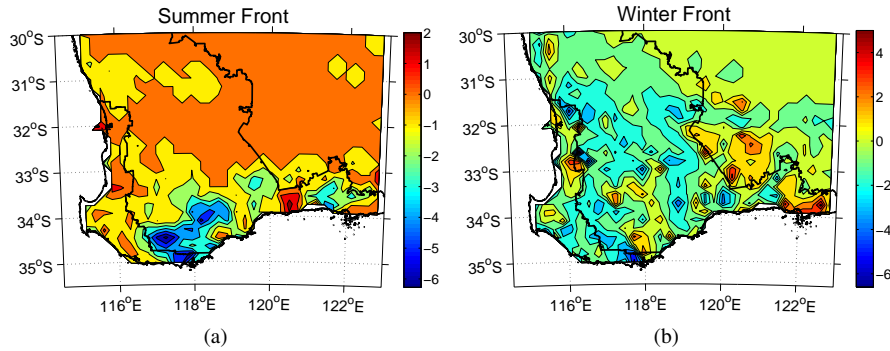


Fig. 9 Difference in total surface accumulated precipitation (mm) between current and pre-European vegetation cover for (a) the summer front, integrated from 0900 LST on 9 December 2005 to 0900 LST on 12 December 2005, (b) the winter front, integrated from averaged from 0900 LST on 5 August 2007 to 0900 LST on the 8 August 2007.

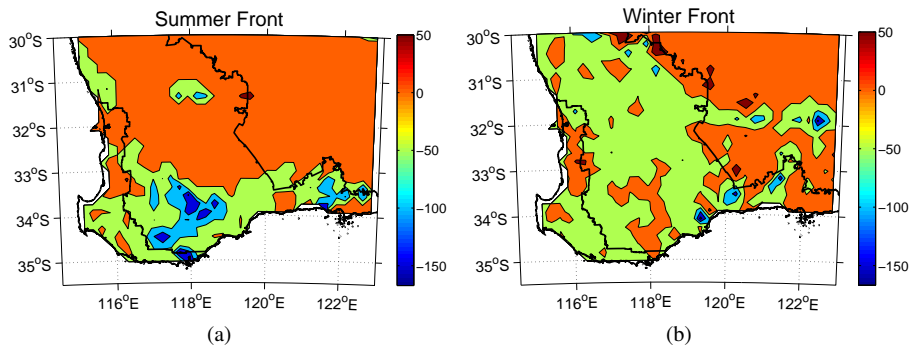


Fig. 10 Same as in Fig. 9 except showing the percentage difference (ΔP in Eq. 1).

Given that there is no additional source of atmospheric moisture and the only difference is a change in land-cover, the increase in precipitation under pre-European land cover must be due to enhanced vertical motion and cloud micro-physical processes. That is, there must be a mechanism bringing additional moisture beyond the lifting condensation level or the freezing level, which would enhance convective cloud formation and increase the likelihood of rain. This is illustrated in Fig. 11 showing the difference in turbulent kinetic energy (TKE) between current and pre-European vegetation cover along a north-south transect passing through 117°E (Fig. 1) for the summer and winter fronts respectively. Fig. 11a shows a clear decrease in

TKE under current vegetation conditions extending up to 1.4 km and well above the lifting condensation level (shown by the dotted white line) for the summer front, and up to 0.6 to 0.8 km for the winter front (Fig. 11b). This implies stronger turbulent mixing throughout the boundary layer and extending beyond the lifting condensation level, which would have invariably enhanced convective precipitation processes. The larger decrease in TKE for the summer front (Fig. 11a) as compared to the winter front (Fig. 11b) would have been due to enhanced surface heating during summer, and this is reflected in the higher percentage decrease in precipitation for the summer front (Fig. 10). Fig. 12 is the same as Fig. 11, except that it shows the change in wind speed. The figure clearly shows an increase in wind speed within the first 600-800 m of the atmosphere under current vegetation cover. This would be due to the lower aerodynamic roughness length of the bare soil (summer front) and crops (winter front), compared to pre-European vegetation cover. Hence, land-cover change (i.e., a change from wooded grasslands to bare soil or crops) not only results in a decrease in turbulence, but increases the frontal speed close to the surface, allowing less time for processes leading to convective precipitation to take place. This decrease in turbulence is further illustrated in Fig. 13 showing a decrease in PBL heights under current vegetation of up to 100-250 m for the summer front and 40-100 m for the winter front throughout the wheat-belt, similar to the findings of Huang et al. (1995).

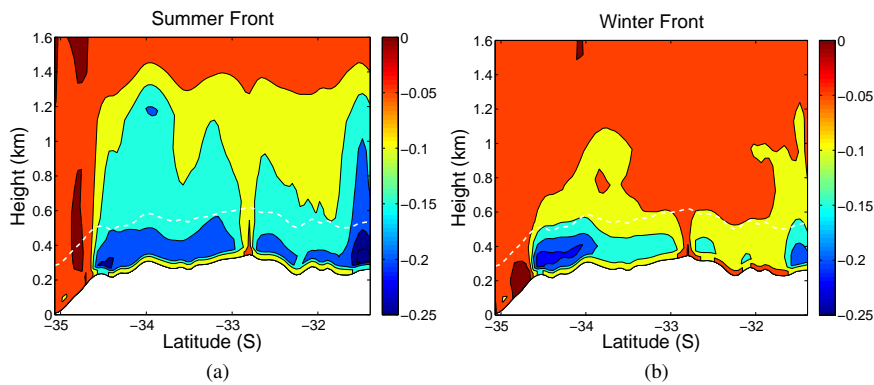


Fig. 11 Difference in turbulent kinetic energy (TKE) ($\text{m}^{-2} \text{s}^{-2}$) along a north-south transect passing through 117°E (Fig. 1) between current and pre-European vegetation cover for (a) the summer front, averaged from 0900 LST on 9 December 2005 to 0900 LST on 12 December 2005, and (b) the winter front, averaged from 0900 LST on 5 August 2007 to 0900 LST on the 8 August 2007. The mean height of the lifting condensation level (LCL) is shown as the dotted white line (the heights of the LCL under current and pre-European vegetation were very similar).

Pitman et al. (2004) argued that the mechanism leading to reduced July precipitation in SWWA due to land-cover change is a change in surface moisture convergence. To test this hypothesis, we define the vertically integrated moisture flux convergence (Φ) following van Zomeren and van Delden (2007) as:

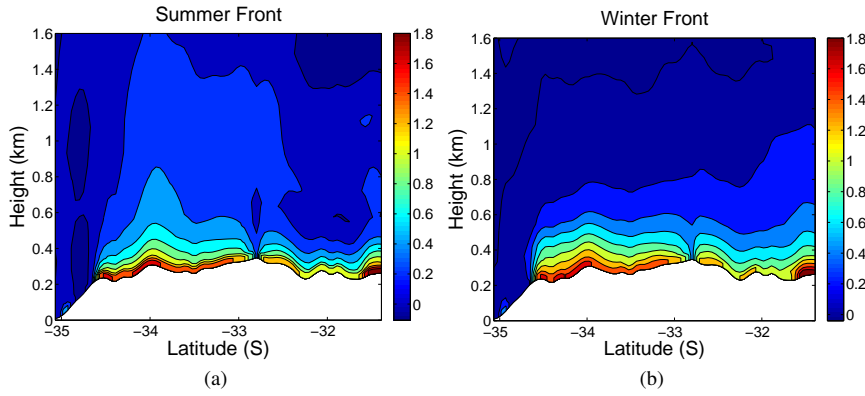


Fig. 12 Same as in Fig. 11 but showing the change in wind speed (m s^{-1}).

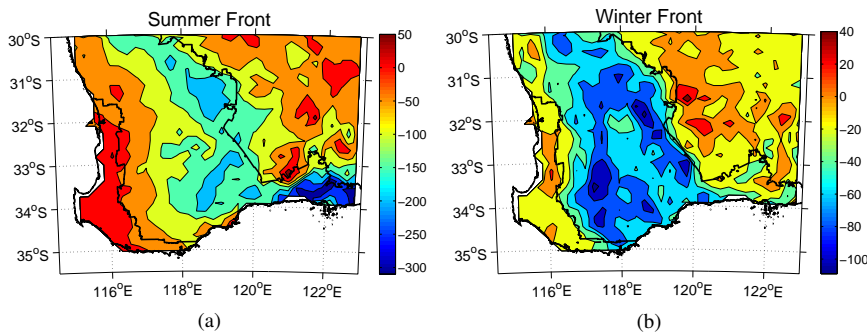


Fig. 13 Difference in planetary boundary layer height (PBL) (m) between current and pre-European vegetation cover for (a) the summer front, averaged from 0900 LST on 9 December 2005 to 0900 LST on 12 December 2005, and (b) the winter front, averaged from 0900 LST on 5 August 2007 to 0900 LST on the 8 August 2007.

$$\Phi = -\frac{1}{g} \int_{700 \text{ hPa}}^{1000 \text{ hPa}} \left(\frac{\delta u q}{\delta x} + \frac{\delta v q}{\delta y} \right) dp \quad (2)$$

where q is the specific humidity, u and v are the zonal (x) and meridional (y) wind components respectively, p is pressure, and g is acceleration due to gravity. Φ is evaluated as the summation of the horizontal moisture flux convergence over the intervals 1000-925, 925-850 and 850-700 hPa. We note that Eq. 2 is the conventional definition of Φ , whereas Pitman et al. (2004) limited their evaluation of moisture convergence to the lowest grid level.

The change in Φ between current and pre-European vegetation cover for the summer and winter front is illustrated in Fig. 14, showing a decrease in Φ along the western boundary of the wheat-belt and an increase further inland, similar to the findings of Pitman et al. (2004). We note however that regions showing a decrease in Φ do not correspond exactly with regions showing a decrease in precipitation (Figs. 9 and 10).

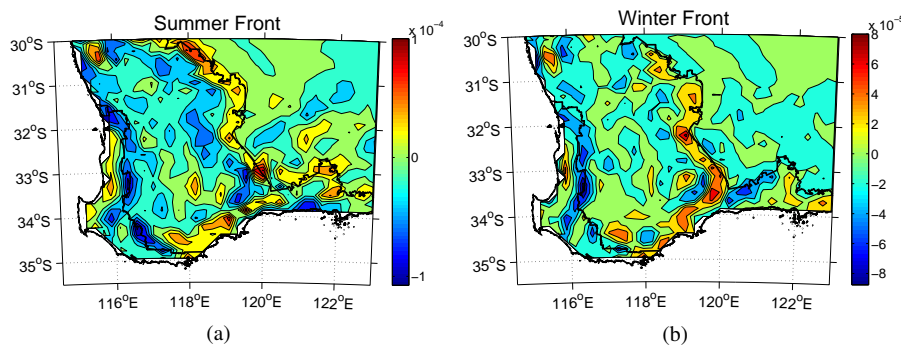


Fig. 14 Same as in Fig. 13 except showing the change in vertically integrated moisture flux convergence (Φ) ($\text{kg m}^{-2} \text{s}^{-1}$).

Given the complexities of land-atmosphere feedbacks, it is likely that the decrease in Φ , together with decrease in TKE and the increase in wind speed provide a plausible mechanism for the decrease in precipitation.

Thus, irrespective of large scale atmospheric changes (e.g., Hope et al. 2006; Nicholls 2010), land-cover change has contributed to a decrease in microphysical processes within frontal systems to decrease precipitation in SWWA. Whilst large scale processes have decreased the number of fronts reaching SWWA, land-cover change has reduced the effectiveness of these frontal systems in producing precipitation (at least for the ones considered here, which are Type 2 systems (Wright 1974) and sensitive to surface conditions). Furthermore, several studies investigating the influence of anthropogenic (greenhouse) forcing on SWWA rainfall (e.g., Cai and Cowan 2006; Timbal et al. 2006) conclude that these alone cannot account for all of the decline in rainfall and other factors (like land-cover change) must be accounted for.

6 Conclusions

RAMS version 6.0 is used to model a summer and a winter cold front in SWWA and shown to reproduce the overall features of the fronts reasonably well, but the quantitative errors are shown to be high. Namely, temperatures are over-predicted by as much as 5 °C as the model does not reproduce the strong temperature gradient between cold and warm air within the front. This is attributed to the coarse resolution of the input boundary conditions and is an inherent limitation of the model setup. The model reproduces the spatial and temporal extent of precipitation well for both fronts, but quantitatively, precipitation is under-predicted along the west coast and over-predicted further inland for the winter front. This is partly attributed to orographic effects which cannot be adequately resolved due to the relatively coarse resolution of the second model grid.

Sensitivity tests are carried out to investigate effects of historical land-cover change and it is found that land-cover change results in a decrease in precipitation for both

fronts, with a higher decrease for the summer front. The decrease in precipitation is attributed to a decrease in turbulent kinetic energy and moisture flux convergence as well as a increase in wind speed within the lower boundary layer. The suggested mechanism is that the enhanced vertical mixing under pre-European vegetation cover, with the decrease in wind speeds close to the ground, enhance microphysical processes leading to increased convective precipitation. The higher decrease in precipitation for the summer front is most likely due to enhanced convection during summer.

Whilst this study was limited to two events, it highlights a significant change in microphysical processes caused by land-cover change. Even without large scale shifts in the climate, local land use practices impact on the atmospheric processes and need to be adequately managed under a changing climate.

Acknowledgements The NOAA_OL_SST_V2 data were provided by the NOAA /OAR / ESRL PSD, Boulder, Colorado, USA, from their Web site at <http://www.cdc.noaa.gov/>. All RAMS simulations were supported by iVEC (<http://www.ivec.org>) through the use of advanced computing resources provided by the Australian Resources Research Centre Facility located at Technology Park, Perth. The radiosonde observations were acquired using the National Center for Atmospheric Research Mobile Global Positioning System Advanced Upper-Air Sounding System with support from the National Science Foundation Grant ATM 0523583 and the Australian Research Council's Discovery funding scheme (Project DP0664515). The Australian Soil Water Availability Project soil moisture data were provided by Peter Briggs and Michael Raupach from the Commonwealth Scientific and Industrial Research Organisation division of Marine and Atmospheric Research. Yuling Wu from the University of Alabama in Huntsville assisted with initialising RAMS with the soil moisture data. Jatin Kala is supported by an Australian Post-Graduate Award at Murdoch University, Perth, Western Australia. The comments anonymous reviewers helped improve the manuscript. All of this assistance is gratefully acknowledged.

References

- Allan RJ, Haylock MR (1993) Circulation features associated with the winter rainfall decrease in southwestern Australia. *J Clim* 6:1356–1367
- Anthes R (1984) Enhancement of convective precipitation by mesoscale variations in vegetative covering in semiarid regions. *J Clim Appl Meteorol* 23:541–554
- AUSLIG (1990) Australian Surveying and Land Information Group. Atlas of Australian Resources: Vegetation. Commonw. of Aust., Canberra, ACT. 64 pp.
- Bates BC, Hope P, Ryan B, Smith I, Charles S (2008) Key findings from the Indian Ocean Climate Initiative and their impact on policy development in Australia. *Climatic Change* 89:339–354
- Cai W, Cowan T (2006) SAM and regional rainfall in IPCC AR4 models: Can anthropogenic forcing account for southwest Western Australian winter rainfall reduction? *Geophys Res Lett* 33:L24708, DOI 10.1029/2006GL028037
- Cai XM, Steyn DG (2000) Modelling study of sea breezes in a complex coastal environment. *Atmos Environ* 34:2873–2885
- Cotton WR, Pielke RA (2007) Human impacts on weather and climate. Cambridge University Press, 308 pp.
- Cotton WR, Pielke RA, Walko RL, Liston GE, Tremback CJ, Jiang H, McAnelly RL, Harrington JY, Nicholls ME, Carrio GG, McFadden JP (2003) RAMS 2001: Current status and future directions. *Meteorol Atmos Phys* 82:5–29

- England MH, Ummenhofer CC, Santoso A (2006) Interannual rainfall extremes over southwest Western Australia linked to Indian Ocean climate variability. *J Clim* 19:1948–1969
- Esau IN, Lyons TJ (2002) Effect of sharp vegetation boundary on the convective atmospheric boundary layer. *Agric For Meteorol* 114:3–13
- Gentili J (1971) *Australian Climate Patterns*. Thomas Nelson (Australia) Limited, 285 pp.
- Gero AF, Pitman AJ (2006) The impact of land cover change on a simulated storm event in the Sydney basin. *J Appl Meteorol Clim* 45:283–300
- Gero AF, Pitman AJ, Narisma GT, Jacobson C, Pileke RA (2006) The impact of land cover change on storms in the Sydney Basin, Australia. *Global and Planetary Change* 54:57–78
- Harrington JY (1997) The effects of radiative and microphysical processes on simulated warm and transition season Arctic stratus. Ph.D. dissertation, Atmospheric Science Paper 637. PhD thesis, Colorado State University, 289 pp
- Hope PK, Drosowsky W, Nicholls N (2006) Shifts in the synoptic systems influencing southwest Western Australia. *Clim Dyn* 26:751–764
- Huang X, Lyons TJ, Smith RCG (1995) Meteorological impact of replacing native perennial vegetation with annual agricultural species. *Hydrol Processes* 9:645–654
- Hutchinson MF, Stein JA, Stein JL (2009) GEODATA 9 Second Digital Elevation Model (DEM-9S) Version 3. Online at <http://www.ga.gov.au/>
- IOCI (2002) Indian Ocean Climate Initiative (IOCI) - Climate variability and change in southwest Western Australia. Online at http://www.ioci.org.au/pdf/IOCI_TechnicalReport02.pdf. Accessed 22.10.2009
- Kain JS, Fritsch JM (1993) Convective parameterisation for mesoscale models: The Kain-Fritsch scheme, in *The Representation of Cumulus Convection in Numerical Models*, edited by A. Emanuel and D. J. Raymond, pp. 165-170., Am. Meteorol. Soc., Boston, Mass.
- Kala J, Lyons TJ, Abbs DJ, Nair US (2010) Numerical simulations of the impacts of land-cover change on a southern sea breeze in south-west Western Australia. *Boundary-Layer Meteorol* 135:485–503
- Kanae S, Oki T, Musiak K (2001) Impact of deforestation on regional precipitation over the Indochina peninsula. *J Hydrometeorol* 2:51–70
- Kotroni V, Lagouvardos K, Kallos G (1998) Modelling study of the IOP2 cold front of the FRONTS 87 experiment. *Meteorol Appl* 5:297–306
- Lyons TJ (2002) Clouds prefer native vegetation. *Meteorol Atmos Phys* 80:131–140
- Lyons TJ, Schwerdtfeger P, Hacker JM, Foster IJ, Smith RCG, Huang X (1993) Land-atmosphere interaction in a semiarid region: the bunny fence experiment. *Bull Am Meteorol Soc* 16:551–558
- Lyons TJ, Smith RCG, Huang X (1996) The impact of clearing for agriculture on the surface energy balance. *Int J Clim* 16:551–558
- Ma Y, Lyons TJ (2000) Numerical simulation of a sea-breeze under dominant synoptic conditions at Perth. *Meteorol Atmos Phys* 73:89–103
- Mellor GL, Yamada T (1982) Development of a turbulence closure model for geophysical fluid dynamics problems. *Rev Geophys Space Phys* 20:851–875

- Meyers MP, Walko RL, Harrington JY, Cotton WR (1997) New RAMS cloud microphysics parameterization. Part II: The two-moment scheme. *Atmos Res* 45:3–39
- Miao JF, Kroon LJM, de Arellano JVG, Holtslag AAM (2003) Impacts of topography and land degradation on the sea breeze over eastern Spain. *Meteorol Atmos Phys* 84:157–170
- Nair US, Hjelmfelt MR, Pielke RA (1997) Numerical simulation of the 9–10 June 1972 Balck Hills storm using CSU RAMS. *Mon Weather Rev* 125:1753–1766
- Nicholls N (2010) Local and remote causes of the southern Australian autumn–winter rainfall decline 1958–2007. *Clim Dyn* 34:835–845
- Peel DR, Pitman AJ, Hughes LA, Narisma GT, Pielke RA (2005) The impact of realistic biophysical parameters for eucalypts on the simulation of the January climate of Australia. *Environ Modell Software* 20:595–612
- Pielke RA (2001) Influence of the spatial distribution of vegetation and soils on the prediction of cumulus convective rainfall. *Rev Geophys* 39:151–177
- Pielke RA, Cotton WR, Walko RL, Tremback CJ, Lyons WA, Grasso LD, Nicholls ME, Moran MD, Wesley DA, Lee TJ, Copeland JH (1992) A comprehensive meteorological modelling system–RAMS. *Meteorol Atmos Phys* 49:69–91
- Pielke RA, Walko RL, Steyaert LT, Vidale PL, Liston GE, Lyons WA, Chase TN (1999) The influence of anthropogenic landscape changes on weather in south Florida. *Mon Weather Rev* 127:1663–1673
- Pielke RA, Adegoke J, Beltrán-Przekurat A, Hiemstra CA, Lin J, Nair US, Niyogi D, Nobis TE (2007) An overview of regional land use and land cover impacts on rainfall. *Tellus B* 59:587–601
- Pitman AJ, Narisma GT, Pielke RA, Holbrook NJ (2004) Impact of land cover change on the climate of southwest Western Australia. *J Geophys Res* 109:D18109
- Pitts RO, Lyons TJ (1989) Airflow over a two-dimensional escarpment. I: Observations. *Q J Roy Meteorol Soc* 115:965–981
- Pitts RO, Lyons TJ (1990) Airflow over a two-dimensional escarpment. II: Hydrostatic flow. *Q J Roy Meteorol Soc* 116:363–378
- Raupach MR, Briggs PR, Haverd V, King EA, Paget M, Trudinger CM (2008) Australian Water Availability Project. CSIRO Marine and Atmospheric Research, Canberra, Australia. <http://www.csiro.au/awap>. Accessed 22.10.2009
- Raupach MR, Briggs PR, Haverd V, King EA, Paget M, Trudinger CM (2009) Australian Water Availability Project (AWAP): CSIRO Marine and Atmospheric Research Component: Final Report for Phase 3. CAWCR Technical Report No. 013. 67 pp.
- Reynolds RW, Rayner NA, Smith TM, Stokes DC, Wang W (2002) An improved in situ and satellite SST analysis for climate. *J Clim* 15:1609–1625
- Ryan BF, Katzfey JJ, Abbs DJ, Jakob C, Lohmann U, Rockel B, Rotstayn LD, Stewart RE, Szeto KK, Tselioudis G, Yau MK (2000) Simulations of a cold front by cloud-resolving, limited-area, and large-scale models, and a model evaluation using in situ and satellite observations. *Mon Weather Rev* 128:3218–3235
- Samuel JM, Verdon DC, Sivapalan M, Franks SW (2006) Influence of Indian Ocean sea surface temperature variability on southwest Western Australian winter rainfall. *Water Resour Res* 42:W08402, DOI 10.1029/2005WR004672

-
- Smagorinsky JS (1963) General circulation experiments with primitive equations. I. The basic experiment. *Mon Weather Rev* 91:99–164
- Smith IN, McIntosh P, Ansell TJ, Reason CJC, McNinnes K (2000) Southwestern Western Australian winter rainfall and its association with Indian Ocean climate variability. *Int J Clim* 20:1913–1930
- Sturman A, Tapper N (1996) *Climate and weather of Australia and New Zealand*. Oxford University Press, 476 pp.
- Timbal B, Arblaster JM, Power S (2006) Attribution of the late 20th century rainfall decline in South-West Australia. *J Clim* 19:2046–2067
- Walko RL, Cotton WR, Meyers MP, Harrington JY (1995) New RAMS cloud microphysics parameterization. Part I: The single-moment scheme. *Atmos Res* 38:29–62
- Walko RL, Band LE, Baron J, Kittel TGF, Lammers R, Lee TJ, Ojima D, Pielke RA, Taylor C, Tague C, Tremback CJ, Vidale PL (2000) Coupled atmosphere-biosphere-hydrology models for environmental modeling. *J Appl Meteorol* 39:931–944
- Wright PB (1974) Seasonal rainfall in Southwestern Australia and the general circulation. *Mon Weather Rev* 102:219–232
- van Zomeren J, van Delden A (2007) Vertically integrated moisture flux convergence as a predictor of thunderstorms. *Atmos Res* 83:435–445